GEOPHYSICAL RESEARCH LETTERS, VOL. 36, L10603, doi:10.1029/2009GL037620, 2009

Significance of Langmuir circulation in upper ocean mixing: Comparison of observations and simulations

T. Kukulka,[1,2] A. J. Plueddemann,[1] J. H. Trowbridge,[2] and P. P. Sullivan[3]

Received 4 February 2009; revised 27 March 2009; accepted 20 April 2009; published 28 May 2009.

[1] Representing upper ocean turbulence accurately in models remains a great challenge for improving weather and climate projections. Langmuir circulation (LC) is a turbulent process driven by wind and surface waves that plays a key role in transferring momentum, heat, and mass in the oceanic surface layer. We present a direct comparison between observations and large eddy simulations, based on the wave-averaged Navier-Stokes equation, of an LC growth event. The evolution of cross-wind velocity variance and spatial scales, as well as mixed layer deepening are only consistent with simulations if LC effects are included in the model. Our results offer a validation of the large eddy simulation approach to understanding LC dynamics, and demonstrate the importance of LC in ocean surface layer mixing. **Citation:** Kukulka, T., A. J. Plueddemann, J. H. Trowbridge, and P. P. Sullivan (2009), Significance of Langmuir circulation in upper ocean mixing: Comparison of observations and simulations, *Geophys. Res. Lett.*, *36*, L10603, doi:10.1029/2009GL037620.

1. Introduction

[2] Mixing in the ocean surface layer plays a key role in weather and climate systems, because it couples the ocean and atmosphere through air-sea fluxes of heat, momentum, and mass [*Jahne and Haussecker*, 1998; *Melville*, 1996; *Thorpe*, 2004]. Understanding the turbulent processes involved in surface layer mixing remains one of the great challenges in modeling the coupled ocean-atmosphere system. Ocean surface waves influence upper ocean turbulence because greater below-crest and smaller below-trough wave orbital speeds induce a residual circulation (Stokes drift) that tilts vertical vorticity into the direction of wave propagation [*Craik and Leibovich*, 1976]. This vortex tilting interacts with sheared surface currents to form wind-aligned roll vorticies, called Langmuir circulation (LC) [*Langmuir*, 1938]. LC is an insufficiently understood turbulent process that is not represented in most upper ocean models, despite the fact that LC may be a principal component of upper ocean mixing [*Leibovich*, 1983; *Thorpe*, 2004]. LC impacts a broad range of oceanographic problems, such as the propagation of acoustic signals [*Smith*, 1989; *Zedel and Farmer*, 1991], the dispersion of oil spills and other surfactants [*McWilliams and Sullivan*, 2000; *Thorpe*, 2000], the resuspension and transport of sediments in a coastal ocean [*Gargett et al.*, 2004], and the distribution of plankton and nutrients within the photic zone [*Denman and Gargett*, 1995].

[3] The seminal paper by Langmuir first described counter-rotating roll vortices within the ocean surface layer, based on observations of floating bands of seaweed [*Langmuir*, 1938]. Laboratory experiments by *Faller* [1978] supported a generation mechanism based on wave-current interactions, which has been described in a systematic mathematical theory by *Craik and Leibovich* [1976]; the full three dimensional current pattern of Langmuir circulation was observed directly by *Weller et al.* [1985]. Throughout the 1990s, novel sensing techniques provided improved understanding of Langmuir circulation characteristics, as well as growth and decay of the circulation with wind and wave conditions [*D'Asaro and Dairiki*, 1997; *Farmer and Li*, 1995; *Plueddemann et al.*, 1996; *Smith*, 1992]. During the same period, a computational approach based on turbulence resolving large eddy simulations (LES) of the Craik-Leibovich (CL) equations was used to investigate the properties of Langmuir circulation [*Li et al.*, 2005; *McWilliams et al.*, 1997; *Skyllingstad and Denbo*, 1995].

[4] While Langmuir circulation is now accepted as a fundamental surface layer mixing process, there is an ongoing debate as to whether Langmuir circulation contributes directly to mixed layer deepening and whether it is appropriately parameterized in surface layer models [*Li et al.*, 1995]. The principal challenge in interpreting observations and model results is the scarcity of direct comparisons between observed and modeled Langmuir circulation features. This study connects cutting-edge observations to state-of-the art modeling by presenting a direct comparison of observed and modeled Langmuir circulation growth. Our results offer a critical validation of the LES modeling approach to the Langmuir circulation problem and demonstrate the importance of Langmuir circulation in ocean surface layer mixing.

2. Methods

2.1. Wind Event During SWAPP Experiment

[5] The Surface Waves Processes Program (SWAPP) was conducted in the Pacific Ocean about 550 km west off the California Coast during February and March of 1990 [*Plueddemann et al.*, 1996; *Smith*, 1992]. The SWAPP data set provides comprehensive measurements of a) ocean surface wave fields; b) heat and momentum air-sea fluxes; c) vertical profiles of temperature, salinity, and currents; as well as d) unique subsurface turbulence estimates from "LC detectors" (discussed below). The measurement setting at times resembles closely the idealized open ocean conditions

[1]Department of Physical Oceanography, Woods Hole Oceanographic Institution, Woods Hole, Massachusetts, USA.
[2]Department of Applied Ocean Physics and Engineering, Woods Hole Oceanographic Institution, Woods Hole, Massachusetts, USA.
[3]National Center for Atmospheric Research, Boulder, Colorado, USA.

0094-8276/09/2009GL037620$05.00

often assumed in LES studies. We focus our analysis on a single 3 h wind event from 7:00AM to 10:00AM (PST) on March 4, when wind and waves were approximately unidirectional and aligned. The wind speed at 10 m height increased from U_{10} = 8 ms^{-1} at 7:00AM to 13 ms^{-1} at 8:00AM and then weakened again to about 10 ms^{-1}. The significant wave height weakly developed from H_s = 2.6 m to 2.9 m. The surface heat fluxes changed from cooling between 60–90 Wm^{-2} to warming around 9:00AM and approached a value of 200 Wm^{-2} at 10:00AM. Since the magnitude of the Monin-Obukhov length exceeds 100 m, which is much larger than the order 10 m deep mixed layer, buoyancy effects are likely to play a secondary role in the upper ocean turbulence dynamics. From 7:30AM to 9:00AM observations indicate that larger scale advective processes played a relatively small role in the near surface ocean temperature evolution between depths of 7 m and 27 m [*Smith*, 1992].

[6] The LC detectors consist of special purpose acoustic instruments that measure horizontal velocities of surface trapped bubbles over a horizontal range of a few hundred meters [*Smith*, 1989; *Zedel and Farmer*, 1991]. In the presence of LC, sonar beams oriented perpendicular to the wind direction (''cross-wind'') detect horizontal bands due to velocity convergence zones of coherent surface LC structures. In order to compare measurements with model results, it is necessary to understand the vertical extent of these surface measurements. The near surface bubble distribution decreases roughly exponentially in the vertical with a decay scale around 1.0 to 1.5 m and confines the vertical extent of the measurement volume to about 3 m, depending on wind and wave conditions. These measurements are invaluable in diagnosing model results as well as in setting up the model initial, boundary, and forcing conditions.

2.2. Model Setup

[7] We employ the laterally periodic LES model described by *McWilliams et al.* [1997]. This model solves the CL equation spatially averaged over the subgrid scale (SGS). The CL momentum equations capture LC dynamics by a vortex force that involves the Stokes drift. If the Stokes drift is set to zero, the LES model simply solves the spatially averaged Navier-Stokes equations without wave forcing, but still captures shear and buoyancy instabilities (''no LC'' model). Turbulent SGS fluxes are parameterized via an SGS eddy viscosity that depends on the SGS turbulent kinetic energy (TKE). The SGS TKE, in turn, is determined from a prognostic equation [*Moeng*, 1984]. Closer to the ocean surface the SGS model is modified for better correspondents with Monin-Obukhov similarity theory [*Sullivan et al.*, 1994]. At the ocean surface, time varying heat and momentum fluxes are specified based on the observations. An internal-gravity-wave radiation condition is imposed at the bottom of the computational domain.

[8] The initial fields of velocity, temperature, and SGS energy were obtained in two stages. First, a fully developed turbulent flow field with water friction velocity $u_* = 6 \times 10^{-3}$ ms^{-1} (corresponding to $U_{10} \approx 5$ ms^{-1}, roughly consistent with the wind speed at the onset of the modeled event) was established during a spin up time of four eddy turnover time scales, each approximated by h/u_*. The initial temperature was set constant to a depth h = 30 m below which the temperature decreased at a rate of 0.01°C m^{-1}. Consistent with previous LES studies [*Li et al.*, 2005; *McWilliams et al.*, 1997], the simulated fields approximately reached a stationary state in this first stage. In the second initialization stage, the simulated fields adjusted to the observed forcing. Temperature profile data, which are used to set up the initial conditions, were obtained from vector-measuring current meters (VMCMs) and from conductivity-temperature depth instruments (CTDs). The initial temperature profiles are taken from the VMCM data because these data are closer to the surface with the shallowest measurement at z = 2.25 m. For comparison of observed and simulated temperature profiles during the 3 h event (discussed below), we use the CTD data because these are sampled with higher vertical resolution. The stratification across the MLD (e.g. from 6 to 12 m depth) is comparable for the VMCM and CTD profiles (e.g., 0.016°C/m and 0.014°C/m, respectively at 6:30AM) although the more highly resolved CTD profile has stronger local gradients. The temperature profile measured at 6:30AM was imposed and the simulation was forced for 1 h with air-sea flux data obtained from 5:30AM to 6:30AM (roughly two eddy turnover periods, strong temperature gradients were at about 8 m depth), so that the turbulent fields could adjust to the observed temperature profile. Based on these results the temperature field was reinitialized with the measured 6:30AM profile and observed fields from 6:30AM to 10:00AM were simulated by imposing the observed surface fluxes and wave forcing in the LC case. The time dependent Stokes drift in the CL equations has been estimated based on a monochromatic surface wave whose amplitude and frequency is consistent with the significant wave height and dominant frequency obtained from observed time dependent wave height spectra. The turbulent Langmuir number $La_t = (u_*/v_s)^{1/2}$ is between La_t = 0.3 and 0.6 during the wind event, here v_s denotes the surface Stokes drift. According to the turbulence regime diagram from *Li et al.* [2005], the turbulence investigated here is mainly driven by surface waves through LC instabilities.

[9] Our default model domain spans a 200 m × 200 m horizontal and 60 m deep ocean volume with 256 × 256 horizontal and 150 vertical grid points, i.e., the grid resolution is $\Delta x \approx 0.78$ m in the horizontal and Δz = 0.4 m in the vertical. This grid resolves the flux and energy carrying eddies. A relatively high grid resolution is particularly important without LC, in order to capture small scale stratified turbulence, which results from Kelvin-Helmholtz type instabilities and accomplishes mixing near the thermocline [*Beare et al.*, 2006; *Ivey et al.*, 2008; *Skyllingstad et al.*, 2000]. Without LC (the more challenging simulation, as eddies are smaller) we also ran the experiment on a 100 m × 100 m × 45 m domain with 250 × 250 × 150 and 128 × 128 × 75 grid points. These and other sensitivity experiments with different domain and grid sizes indicate that a higher resolution and a larger domain does not significantly change the results presented here.

3. Results

3.1. Surface Cross-Wind Velocity Variation

[10] Because the surface cross-wind velocity variance, σ_v^2, is relatively large in the presence of LC compared to

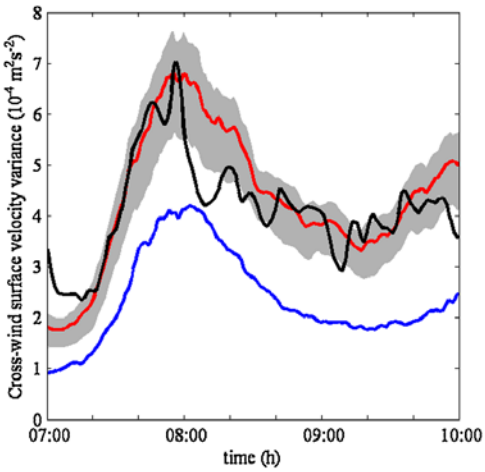

Figure 1. Comparison of observed surface cross-wind velocity variance (black line) and simulations at z = 1.4 m with LC (red lines) and without LC (blue line). Gray area indicates range of LC results between depths of z = 1.0 m to z = 2.2 m, corresponding roughly to the major instrumental depth range response due to a variable bubble layer. Without LC results are approximately vertically homogeneous over the extent of the bubble layer.

solid wall boundary layer turbulence, it serves as an important diagnostic variable [*Li et al.*, 2005; *McWilliams et al.*, 1997]. Simulated σ_v^2 are calculated based on horizontal averages at each time point and depth level. With LC, modeled σ_v^2 at z = 1.4 m (red line in Figure 1), corresponding roughly to the mid bubble layer depth, tracks well the measurements from *Smith* [1992] (black line), while without LC the velocity variance is underestimated (blue line). Model results with LC for depths between z = 1.0 m and 2.2 m (gray area) roughly encompass the measurements. Part of the observed variability is due to instrument noise, estimated between 1.6 and 2.0 $\times$ 10^{-4} m^2 s^{-2}, but also due to variations in the bubble layer depth. Without LC, modeled σ_v^2 are nearly homogeneous over the first few meter depth and well represented by the model result from z = 1.4 m in Figure 1. This comparison of observed and simulated σ_v^2 indicates that simulations with LC capture important features of upper ocean turbulence dynamics and motivates a closer look at the evolution of length scales contributing to σ_v^2.

[11] Similar to the observational data analysis, modeled surface cross-wind velocity (v) spectra are calculated based on Fourier transforms of v taken along the cross-wind direction (roughly coinciding with the sonar beam direction of the LC detector). Data processing for the LES differs from the observational analysis in that we average Fourier transforms along the wind direction rather than over time and that we are able to resolve multiple depth levels. Consistent with our foregoing analysis we present here modeled spectra at a depth of z = 1.4 m.

[12] Based on the observations, we distinguish between four LC development phases: 1) weak LC activity, 2) initial LC development, 3) LC growth, and 4) developed LC (Figure 2a). During phase 1) the simulations indicate relatively weak LC activity with σ_v^2 close to the noise level of observations (Figure 2b). *Smith* [1992] discusses in detail this somewhat surprising weak LC activity, given wind speeds of U_{10} = 8 ms^{-1} and significant wave heights of H_s = 2.6 m; and a possible explanation is provided by *Phillips* [2001]. During phase 2), significant LC activity can be detected roughly 15 min after the wind increased to 13 ms^{-1} around 7:40am. At about 7:40am the first signifi-

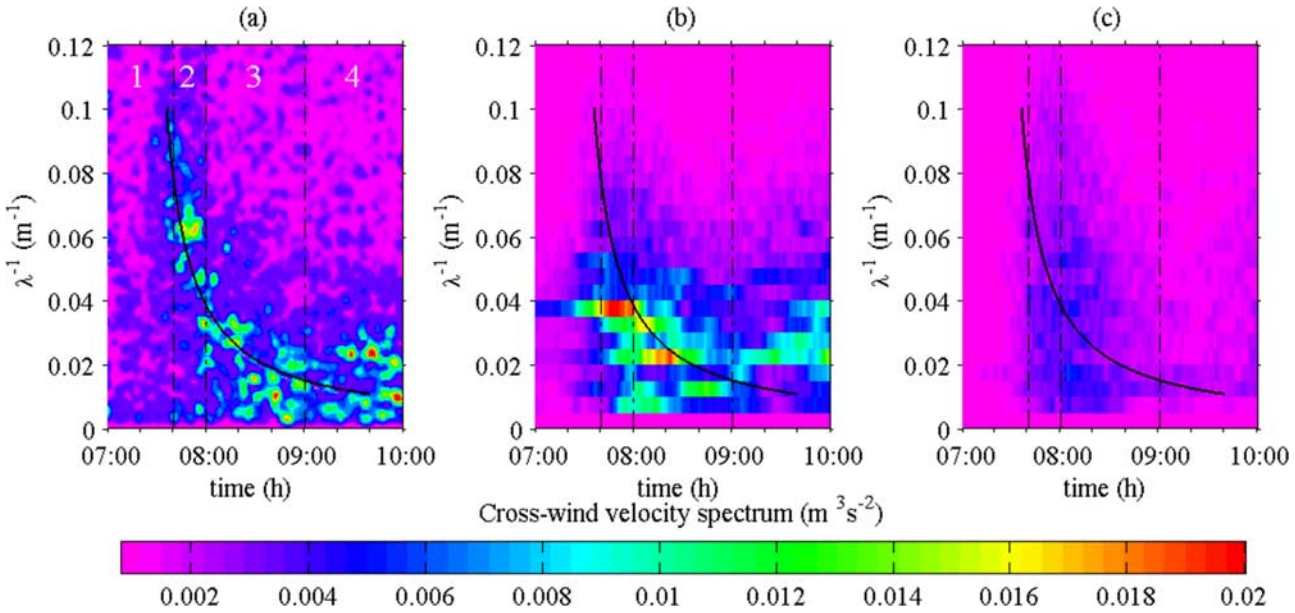

Figure 2. Evolution of cross-wind velocity spectra: (a) observations, simulations (b) with and (c) without Langmuir circulation. The solid black line corresponds to a length scale increase of 40 mh^{-1} (subjectively determined by *Smith* [1992]). λ^{-1} denotes the wavenumber and λ is the wavelength. Dashed-dotted lines separate four LC development phases, as described in the main text: 1) weak LC activity, 2) initial LC development, 3) LC growth, and 4) developed LC.

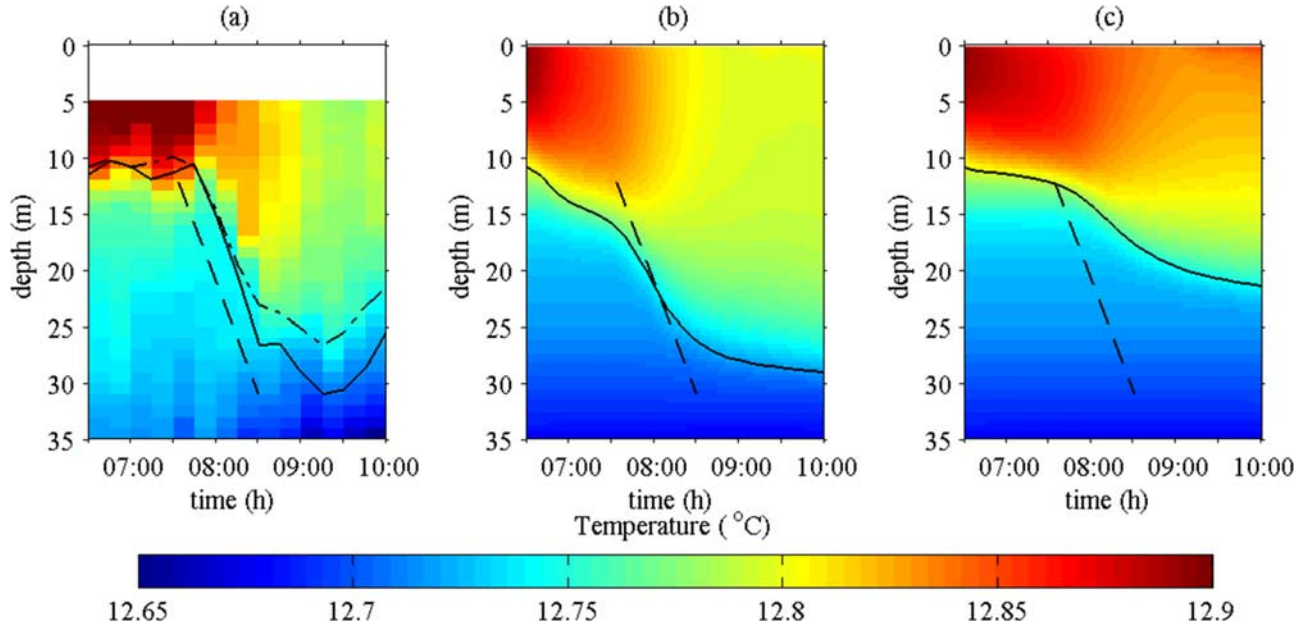

Figure 3. Evolution of temperature profiles: (a) observations, simulations (b) with and (c) without Langmuir circulation. The mixed layer depth (solid line) increases more greatly in the LC case. The observed rate of mixed layer deepening has been previously estimated as 20 mh^{-1} (dashed lines at the identical time depth locations in each plot). The dash-dotted line in Figure 3a shows less accurate MLD estimates based on the VMCM data with coarser vertical resolution.

cant local spectral maximum in time-wavenumber domain appears with an observed peak wavenumber at $\lambda_{max}^{-1} \approx 0.06$ m^{-1} and a simulated one at $\lambda_{max}^{-1} \approx 0.04$ m^{-1}, corresponding to an observed and simulated LC cell size of $\lambda_{max}/2 \approx 8$ m and 12 m, respectively. A possible reason for this difference is that the mixed layer, which confines the spatial extent of LC, deepens at different rates for the observed and simulated cases (see below). Note that no outstanding scale can be observed in the simulated no-LC case during phases 2 and 3 (Figure 2c). During LC growth (phase 3), the observed and modeled LC scales increase over approximately 1 h to wavenumbers at $\lambda^{-1} \approx 0.02$ m^{-1}, supporting a dominant scale from streak to streak of about 50 m that has been observed [*Smith*, 1992]. A reference curve with constant growth rate of 40 mh^{-1} is indicated (black lines). In the final developed LC stage (phase 4), length scales are distributed in a wavenumber band between 0.01 $m^{-1} < \lambda^{-1} < 0.04$ m^{-1} with smaller observed wavenumbers.

3.2. Mixed Layer Deepening

[13] We compare 15 min average temperature measurements from a conductivity-temperature depth instrument (CTD), which profiled vertically at approximately 2 min intervals [*Smith*, 1992], with horizontally averaged, instantaneous LES temperature profiles (Figure 3). The mixed layer depth (MLD) is defined as the depth where the temperature decreases by $\Delta T = 0.08$°C from the near surface value at $z = 6.0$ m, which is the shallowest reliable measurement from the CTD. This MLD criterion corresponds to a density difference, $\Delta\sigma_T$, of about 0.016 kg m^{-3} for the observed temperature-salinity range, and was chosen to approximate the $\Delta\sigma_T$ MLD criteria of 0.015 to 0.020 kg m^{-3} used by *Smith* [1992]. Concurrent with the onset of strong LC activity, the mixed layer rapidly deepens from around 7:40AM to 8:30AM. The final MLD is around 28 m in both observations (Figure 3a) and LC simulation (Figure 3b; these values have been obtained by averaging the MLD from 8:30AM to 10:00AM). Without LC (Figure 3c) the onset of the mixed layer deepening, accomplished mainly by shear instabilities, is delayed and the extent of deepening is less, with a final MLD of about 20 m. Since turbulent processes drive mixing, the maximum rate of mixed layer deepening approximately coincides with the maximum σ_v^2 (Figure 1).

[14] Despite good agreement between the observations and the simulation with LC during phase 2–4, it is notable that the simulation shows more rapid MLD deepening during phase 1. Three explanations for this phenomenon are considered. First, the initial temperature profile for the simulations is slightly different from the initial CTD profile shown in Figure 3 (see section 2.2). However, the evolution of MLD from CTD and VMCM temperatures is similar (Figure 3a) and it appears unlikely that the LES results are sensitive to such small differences in initial conditions. Second, observations indicate that during phase 1, winds were veering and not perfectly aligned with the wave field. This could have delayed LC development, and resulting MLD erosion, in the observations relative to the simulation where wind direction is steady and always aligned with the waves. The excellent agreement of observed and modeled σ_v^2 during phase 1 (Figure 1) argues against this explanation. Finally, it is possible that large-scale advective processes not captured in the simulations sustain the observed stratification during the first 30–45 min. of the forcing event. This idea is supported by the fact that MLD in both the LC and no-LC simulation deepen consistently from the start of the event (albeit the latter much more slowly) while the obser-

vations show approximately constant MLD in the presence of increasing wind and wave forcing.

4. Conclusions

[15] We have shown that upper ocean observations of mixed layer deepening, subsurface cross-wind velocity variance, and corresponding turbulent length scales during a wind event are only consistent with simulations if the effect of Langmuir circulation is included in the model. This direct comparison of observed and modeled Langmuir circulation growth validates the modeling approach based on large eddy simulations of the Craik-Leibovich equations. Our results indicate that Langmuir circulation contributes significantly to upper ocean mixing and should be incorporated in surface layer models for better understanding upper ocean processes and enhancing climate and weather projections.

[16] **Acknowledgments.** This research was supported by the Office of Naval Research through grants N00014-09-M-0112 (TK) and N00014-06-1-0178 (AP, JT). TK also received support from a Woods Hole Oceanographic Institution Cooperative Institute for Climate and Ocean Research Postdoctoral Scholarship. Computing resources were provided from the National Center for Atmospheric Research, which is sponsored by the US National Science Foundation. We would like to thank Jerry Smith, Tom Farrar, and Gene Terray for stimulating discussions. Two anonymous reviewers provided constructive comments.

References

Beare, R. J., et al. (2006), An intercomparison of large-eddy simulations of the stable boundary layer, *Boundary Layer Meteorol.*, *118*, 247–272.

Craik, A. D. D., and S. Leibovich (1976), A rational model for Langmuir circulations, *J. Fluid Mech.*, *73*, 401–426.

D'Asaro, E. A., and G. T. Dairiki (1997), Turbulence intensity measurements in a wind-driven mixed layer, *J. Phys. Oceanogr.*, *27*, 2009–2022.

Denman, K. L., and A. E. Gargett (1995), Biological physical interactions in the upper ocean—The role of vertical and small-scale transport processes, *Annu. Rev. Fluid Mech.*, *27*, 225–255.

Faller, A. J. (1978), Experiments with controlled Langmuir circulations, *Science*, *201*, 618–620.

Farmer, D., and M. Li (1995), Patterns of bubble clouds organized by Langmuir circulation, *J. Phys. Oceanogr.*, *25*, 1426–1440.

Gargett, A., et al. (2004), Langmuir supercells: A mechanism for sediment resuspension and transport in shallow seas, *Science*, *306*, 1925–1928.

Ivey, G. N., et al. (2008), Density stratification, turbulence, but how much mixing?, *Annu. Rev. Fluid Mech.*, *40*, 169–184.

Jahne, B., and H. Haussecker (1998), Air-water gas exchange, *Annu. Rev. Fluid Mech.*, *30*, 443–468.

Langmuir, I. (1938), Surface motion of water induced by wind, *Science*, *87*, 119–123.

Leibovich, S. (1983), The form and dynamics of Langmuir circulations, *Annu. Rev. Fluid Mech.*, *15*, 391–427.

Li, M., et al. (1995), Role of Langmuir circulation in the deepening of the ocean surface mixed-layer, *Science*, *270*, 1955–1957.

Li, M., et al. (2005), A regime diagram for classifying turbulent large eddies in the upper ocean, *Deep Sea Res., Part I*, *52*, 259–278.

McWilliams, J. C., and P. P. Sullivan (2000), Vertical mixing by Langmuir circulations, *Spill Sci. Technol. Bull.*, *6*, 225–237.

McWilliams, J. C., et al. (1997), Langmuir turbulence in the ocean, *J. Fluid Mech.*, *334*, 1–30.

Melville, W. K. (1996), The role of surface-wave breaking in air-sea interaction, *Annu. Rev. Fluid Mech.*, *28*, 279–321.

Moeng, C. H. (1984), A large-eddy-simulation model for the study of planetary boundary-layer turbulence, *J. Atmos. Sci.*, *41*, 2052–2062.

Phillips, W. R. C. (2001), On an instability to Langmuir circulations and the role of Prandtl and Richardson numbers, *J. Fluid Mech.*, *442*, 335–358.

Plueddemann, A. J., J. A. Smith, D. M. Farmer, R. A. Weller, W. R. Crawford, R. Pinkel, S. Vagle, and A. Gnanadesikan (1996), Structure and variability of Langmuir circulation during the Surface Waves Processes Program, *J. Geophys. Res.*, *101*, 3525–3543.

Skyllingstad, E. D., and D. W. Denbo (1995), An ocean large-eddy simulation of Langmuir circulations and convection in the surface mixed layer, *J. Geophys. Res.*, *100*, 8501–8522.

Skyllingstad, E. D., et al. (2000), Resonant wind-driven mixing in the ocean boundary layer, *J. Phys. Oceanogr.*, *30*, 1866–1890.

Smith, J. A. (1989), Doppler sonar and surface waves: Range and resolution, *J. Atmos. Oceanic Technol.*, *9*, 149–163.

Smith, J. A. (1992), Observed growth of Langmuir circulation, *J. Geophys. Res.*, *97*, 5651–5664.

Sullivan, P. P., et al. (1994), A subgrid-scale model for large-eddy simulation of planetary boundary-layer flows, *Boundary Layer Meteorol.*, *71*, 247–276.

Thorpe, S. A. (2000), Langmuir circulation and the dispersion of oil spills in shallow seas, *Spill Sci. Technol. Bull.*, *6*, 213–223.

Thorpe, S. A. (2004), Langmuir circulation, *Annu. Rev. Fluid Mech.*, *36*, 55–79.

Weller, R. A., et al. (1985), Three-dimensional flow in the upper ocean, *Science*, *227*, 1552–1556.

Zedel, L., and D. Farmer (1991), Organized structures in subsurface bubble clouds: Langmuir circulation in the open ocean, *J. Geophys. Res.*, *96*, 8889–8900.

T. Kukulka and A. J. Plueddemann, Department of Physical Oceanography, Woods Hole Oceanographic Institution, Clark Laboratory 210A, Woods Hole, MA 02543, USA. (tkukulka@whoi.edu)

P. P. Sullivan, National Center for Atmospheric Research, 3450 Mitchell Lane, Boulder, CO 80301, USA.

J. H. Trowbridge, Department of Applied Ocean Physics and Engineering, Woods Hole Oceanographic Institution, 98 Water Street, Woods Hole, MA 02543, USA.